JOURNAL OF MATERIALS SCIENCE 24 (1989) 2165–2176

Mechanisms of energy dissipation during impact in toughened polyamides: a SEM analysis

FRANCO SPERONI, ENRICO CASTOLDI
SNIA Tecnopolimeri SpA – Via Stabilimenti 11 – 20020 Ceriano Laghetto, Milano, Italy
PIERO FABBRI
SNIA Fibre – Centro Sperimentale – Cesano Maderno, Milano, Italy
TRANQUILLO CASIRAGHI
Consultant – Via St Denis 100 – Sesto S. Giovanni, Milano, Italy

The development of dissipative mechanisms during the fracture of toughened polyamides is investigated by SEM.

A preliminary fractographic analysis is carried out on the ductile fracture surfaces of water conditioned PA 6 specimens. Extensive yielding gives rise to a wide development of shear bands and rumples, depending on the local stress conditions. Then, the stress whitened regions under the ductile fracture surfaces of rubber toughened HI-PA 6 specimens are analysed by SEM. This is made possible by means of a simple technique for the cryogenic dissection of ductile fracture surfaces: sections are cut both transversally and longitudinally with respect to the ductile crack growth direction. Under the ductile fracture surfaces extensive cavitation occurs around the rubbery particles, following preferential and definite shear directions. The presence of cavitation is correlated with the distance below the ductile surfaces. The rumpled morphologies can be directly correlated with cavitation and shear bands occurring inside the whitened regions below ductile fractures. Both the orientation of shear bands on the fracture surfaces of water conditioned PA6 and the cavitation–shear yielding morphologies developed inside the fractured PA–rubber blends comply with an octahedral shear model, common to other polymers (rubber toughened epoxies, for instance) and to ductile metals.

1. Introduction

As is well known, the toughness of polyamides (PA) 6 and 6.6 can be considerably increased by water absorption or by blending with elastomers finely dispersed into the matrix [1–3].

However, much still needs to be clarified about the nature of the dissipative mechanisms in toughened polymers, and about the correlations between such mechanisms – crazing, shear yielding or cavitation – and the microstructures of the materials.

Suitable models, fit for each material tested in such conditions that $\sigma_y < \sigma_b$, should be elaborated as functions of the observed dissipative phenomena.

In rubber toughened polyamides 6 and 6.6, for instance, the fracture surfaces of sharply notched specimens broken at 23° C show a typical "rumpled" morphology, previously described by Flexman [4] and Hahn *et al.* [5, 6]. The rumples lie parallel to the notch, causing discontinuities on surfaces characterized by tufts of highly drawn material.

In the present work the nature of rumples is interpreted as an effect of an octahedral shear mechanism [7] associated with extensive cavitation: this should be due to both the concentration of active stresses inside the matrix (at the "equator" of the rubbery particles) and to shear yielding of the matrix itself. Such a kind of mechanism is described by Yee and Pearson [7, 8] with regard to epoxies toughened with polybutadienic liquid rubbers: the authors experimentally show that matrix shear yielding and cavitation around the rubbery particles are the dissipative mechanisms involved in the ductile fracture processes. The dispersed particles act as stress concentrators and promote a localized shear inside the matrix; as a consequence, shear planes (or shear bands) originate in agreement with the octahedral shear model.

At the same time the bulk strain energy is dissipated by cavitation [9].

A seemingly more complex morphology was observed by Hahn *et al.* [6] on the ductile fracture surfaces of high impact PA–rubber blends subjected to fatigue tests; either "patchy" or "rumpled" surfaces appeared on specimens tested at low or high stress intensity, respectively. Moreover, the patch surfaces show signs of voiding. The authors prove that the rumple spacing is not related to the growth rate

0022–2461/89 $03.00 + .12

(da/dN) of the fatigue crack; this suggests that fatigue damage occurs by microvoid nucleation around the rubber particles and by the subsequent growth and coalescence of these voids. A model based on mechanisms of cavitation by shear in PA 6.6–rubber blends is graphically outlined to explain the rumpled morphology; it goes back to previous studies [10] about cavitation mechanisms occurring in metals.

Finally, the authors show that rumpled morphologies are also present on the fatigue fracture surfaces of water conditioned PA 6.6 homopolymers, if the test temperature exceeds the actual T_g of the water conditioned polymer. It is concluded that the fracture surface micromorphology of PA 6.6 and its blends depends strongly on the viscoelastic state of the polymer.

As reported by Hobbs, Bopp and Watkins [11] the SEM analysis of high impact PA 6.6–Polyethylene-g-maleic anhydride blends shows evidence of extensive plastic deformation on the whole notched fracture surface, coupled with the presence of numerous cavities. This suggests that substantial interfacial debonding and voiding, as well as plastic flow on both PA and PE occur during the fracture.

Cavitation phenomena around the rubber particles and the consequent development of shear bands due to matrix plastic deformation are also described by Ramsteiner [12] and coworkers [13] on PA 6–rubber blends: TEM images of deformed sections suggest that the voids preferentially lie on lines approximately inclined 55° to the tensile direction, in agreement with the assumption for cavitation and shear yielding to be concommitant phenomena. According to the authors, crazing must be excluded as a dissipative mechanism.

On the other hand, Flexman [4] observes extensive shear bands associated with fibrils on the external faces of rubber toughened PA 6.6 specimens, close to the fracture surfaces. By means of a sequence of energy balances, Wu [14] estimates that in such materials about 25% of the impact energy is dissipated by crazing and about 75% by yielding of the PA matrix.

1.1. Aims of the present work

The present work aims to increase the knowledge about the correlations between chemical composition, morphology and mechanical properties in high impact PA–rubber blends.

In fact the current theories about this topic do not fully explain the behaviour of such materials: see for instance the different opinions about the nature of the involved dissipative mechanisms [4, 11, 13–14], or the hypotheses about parameters governing the ductile fracture process-namely the dimensions of rubbery particles, rubber–matrix adhesion, or the interparticle distance [11, 14–16]. On the other hand, a full understanding of such phenomena can be very useful both for an optimization of the mechanical properties of industrial products and for the design and application of articles made with these materials.

This work describes the SEM morphological analysis of specimens of tough PA 6–rubber blends, broken at 23° C by sharply notched Charpy impact test. In the adopted testing conditions ductile fractures developed and stress whitening was observed on the whole fracture surfaces and in a volume of materials below them. In agreement with similar considerations by Hahn *et al.* [6] it is reasonable to postulate a close relationship between a high impact strength and the formation of a stress whitened region.

Thus, internal sections of the fractured specimens were obtained perpendicularly to the ductile fracture surfaces, in order to observe the internal morphologies of the whitened zones and to recognize possible traces of material deformations, directly by SEM analysis.

Such sections were cut both longitudinally and transversally to the ductile fracture surfaces (see section 2.3); thus it was possible to correlate the external morphologies of the ductile fracture surfaces with the stress whitened regions and to study the nature of the principal dissipative mechanisms.

The technique adopted to obtain internal sections, described in detail in section 2.3 (and partly already adopted by Polato [17]) is so simple as to appear even banal: a cryogenic fracture guided by a sharp notch is obtained perpendicularly to the ductile fracture surface. Therefore, the new brittle surfaces show the internal morphology of the previously deformed material. If correctly applied, (the perpendicular fracture propagation must be strictly brittle) this technique allows the unambiguous observation of the inner morphology of the stress whitened regions, without any risk of secondary alterations.

Moreover, it probably can be applied simply to the fractographic study of further heterophase tough blends and, with some precautions, to the failure analysis of reinforced or filled thermoplastics.

2. Experimental details

2.1. Materials

Two different polyamide-based materials were considered in the present work.

(a) Polyamide 6 (PA 6) with the following main characteristics: $\eta_{\text{rel.}} = 3.2$; $\bar{M}\text{n} = 25000\,\text{g mol}^{-1}$; $[\text{NH}_2] = 35\,\text{meq kg}^{-1}$; $[\text{COOH}] = 41\,\text{meq kg}^{-1}$, produced by SNIA TECNOPOLIMERI under the trade name SNIAMID AES 34.

(b) High Impact Polyamide 6 (HI-PA 6), rubber toughened; produced by SNIA TECNOPOLIMERI under the trade name SNIAMID ASN 27 ET.

3PB impact $3.2 \times 12.6 \times 127\,\text{mm}^3$ specimens were injection moulded from materials a and b.

The test bars composed of the pure PA 6 (a) were water conditioned at 90° C for 3 h; then they were stored for ten days in a sealed polyethylene bag to allow homogeneous diffusion of water molecules before testing. Water absorption caused a 4.74% weight increase (measured immediately before testing).

In contrast, the HI-PA 6 injection moulded samples were sealed in polyethylene bags immediately after cooling; they were stored in a dessicator prior to impact testing in the dry state according to the techniques described in the following section. The main standard mechanical properties evaluated for the two materials are summarized in Table I.

TABLE I Main mechanical properties of the considered materials (tested at $T = 23°C$)

Properties	Units	PA 6 SNIAMID AES 34 dry	PA 6 SNIAMID AES 34 cond.	HI-PA 6 SNIAMID ASN 27 ET dry
Water content	%	0.05	4.74	0.10
Flexural modulus	$\mathrm{N\,mm^{-2}}$	2626	637	1570
Izod impact strength	$\mathrm{J\,m^{-1}}$	47.1	1454[a]	991
E_R (rebound modulus)	$\mathrm{N\,mm^{-2}}$	2645	635	1575
σ_y (tensile impact)	$\mathrm{N\,mm^{-2}}$	125	115	60.5
Charpy impact strength[b]	$\mathrm{kJ\,m^{-1}}$	3.71	75	48
K_{IC}(c)	$\mathrm{MN\,m^{1.5}}$	3.71		
$G_{IC}(K_{IC}^2/E)$	$\mathrm{kJ\,m^{-2}}$	5.20		

[a] Specimens bended without complete breakage

[b] 3PB impact with sharp notch

[c] 3PB specimen: 3.2 × 12.7 × 100 mm; a/w = 0,5; impact speed = $1\,\mathrm{m\,sec^{-1}}$

2.2. Fracture technique at 23° C

Sharp notches were machined into the specimens, according to the following procedure: firstly a pre-notch (6 mm depth; 0.5 mm width) was cut by means of a small circular saw, half length of each test bar; then a sharp notch (0.3 mm length) was microtomed at the bottom of the pre-notch with a razor blade. Thus the notched 3PB specimens were characterized by the following parameters: a/w 0.5; $L/w = 8$ (where a = notch depth; b = specimen thickness; L = span; see also Fig. 1).

Charpy impact tests were performed on a CEAST instrumented pendulum (impact speed = $1\,\mathrm{m\,sec^{-1}}$; $T = 23°C$). Figs. 2a to c show some examples of experimental force–deflection curves obtained from different specimens.

2.3. Cold-dissection of the fracture surfaces

HI-PA 6 specimens, previously fractured at room temperature, were horizontally sawn about 1.5 cm below the ductile fracture surfaces; a second sharp notch was machined from the sawn side, perpendicularly to the ductile fracture surface, either transversally or longitudinally oriented as to the ductile crack growth direction.

As previously described (Section 2.2) sharp notches (0.3 mm length) were cut by means of a razor blade at the bottom of a pre-notch (0.5 mm width) cut by a circular saw.

Care was taken in order to avoid any penetration of the notch inside the stress whitened volume caused by impact at 23° C. A 4 mm distance between the sharp notch tip and the ductile fracture surface is a sufficient safety margin to avoid damage to the stress whitened volume.

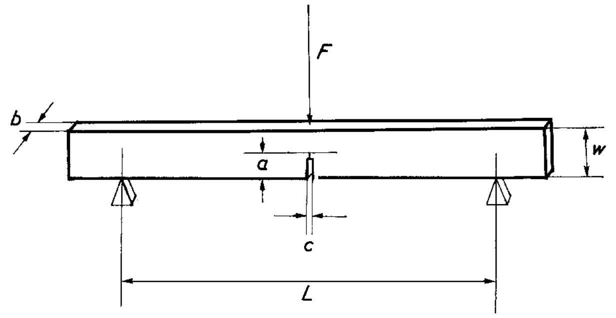

Figure 1 Dimensions of 3PB impact test specimens (a = 6.3 mm, b = 3.2 mm, w = 12.6 mm, c = 0.5 mm, L = 100 mm, a/w = 0.5, L/w = 8).

Then, the specimens were frozen in liquid nitrogen and cryogenically broken: as shown in Fig. 3a, they were placed vertically on the edges of a square hole (9 mm side) cut into a metallic base. Maximum care was taken to limit damages on the ductile fracture surfaces: only the extremity opposite to the notch leaned on the metallic base.

Brittle fractures were obtained by tapping a wedge inserted into the pre-notches by means of a small hammer (see Fig. 3b).

It is very important to be sure that fractures occurred in rigorously brittle conditions; in fact plastic deformations caused by insufficient cooling would change the primary internal morphology caused by the ductile fracture.

A correct use of this simple technique gives rise to longitudinal or transversal brittle fracture surfaces.

For better evidence, Fig. 4 shows the reciprocal orientations of the ductile and brittle fracture planes (indicated by D and B respectively) in correlation with a tern of cartesian axes (x, y, z). Hence, the D surfaces are parallel to the (x, y) plane; the B surfaces are parallel to the (x, z) plane, when transverse to D and to the (y, z) plane when longitudinal to D, respectively.

2.4. Fractography

The D and B surfaces were observed by means of an SEM 515 Philips scanning electron microscope. Every image reports the relative datum-lengths (black and white lines), the applied electric potential (kV) and the magnification. Subsequent numbers are data for the internal catalogue.

3. Experimental results

3.1. Fractographic analysis of water conditioned PA 6

A preliminary analysis was carried out on the ductile fracture surface of a sharply notched PA 6 specimen, toughened by water absorption (see material (a), Section 2.1), in order to collect information about the dissipative mechanisms occurring during crack propagation in polyamides.

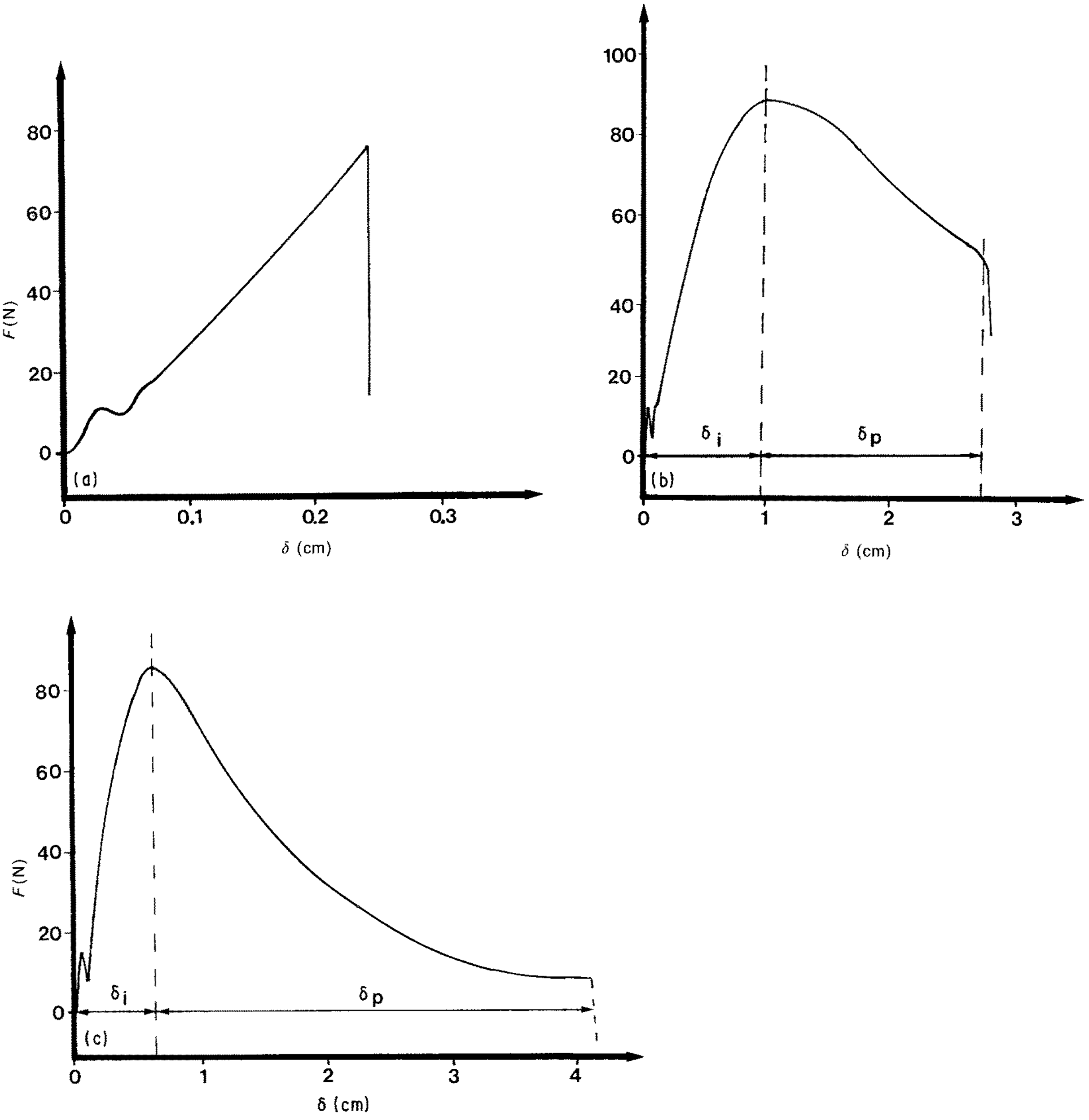

Figure 2 Experimental force (F) against displacement (δ) diagrams obtained by 3PB Charpy impact on sharply notched specimens: (a) Pure PA 6 – dry (H_2O = 0.05%). (b) Pure PA 6 – water conditioned (H_2O = 4.74%). (c) HI-PA 6 – dry (H_2O = 0.10%). (T = 23° C; impact speed = 1 m sec^{-1}; δ_i and δ_p are induction and propagation displacements, respectively.

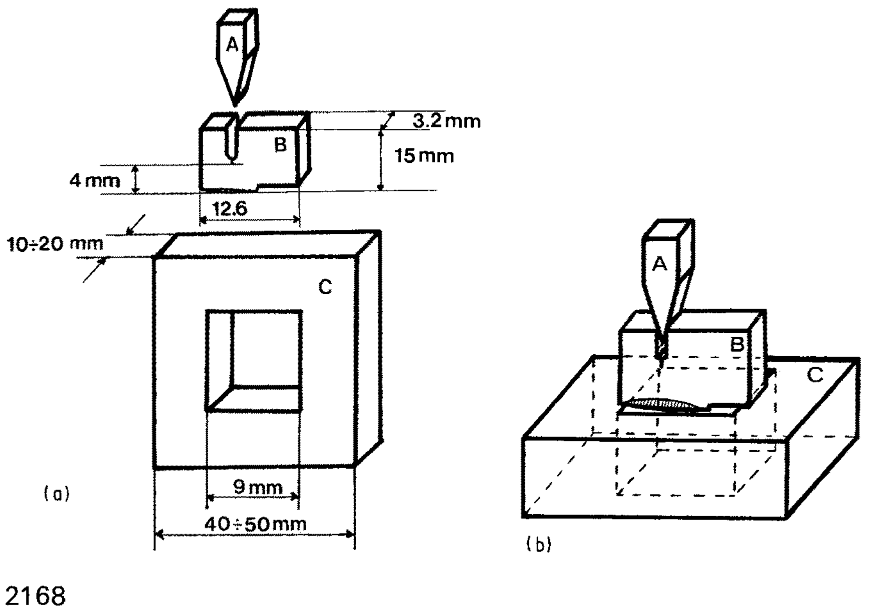

Figure 3 Technique for the transversal cold-dissection of the ductile fracture surfaces. (a) Specimen and base dimensions. (b) Placement of the specimen. (A, wedge, B, specimen, C, Metallic base).

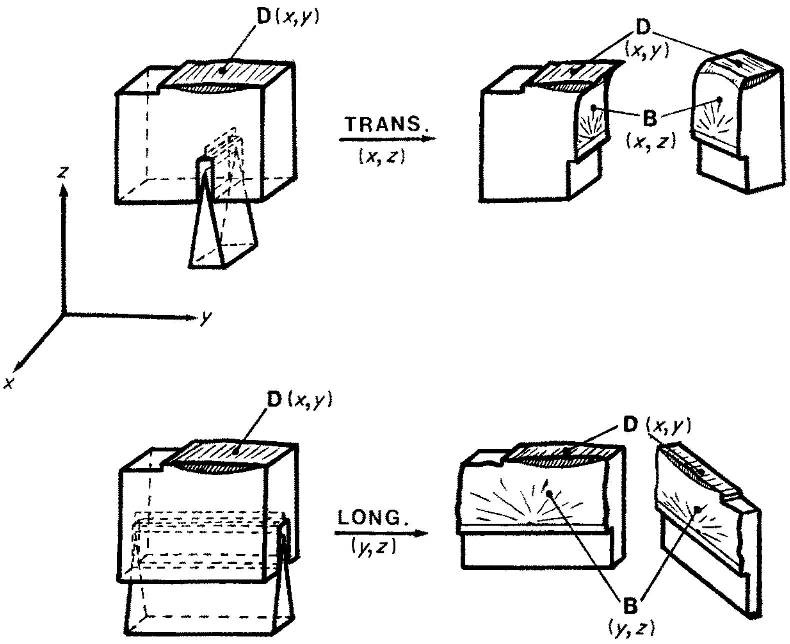

Figure 4 Scheme for the transversal and longitudinal cold-dissection of ductile fracture surfaces of HI-PA 6 (D(x, y) = ductile fracture surfaces at 23° C; B(x, z), B(y, z) = brittle criogenic fracture surfaces).

Fig. 2b shows a force–displacement diagram obtained in accordance with the fracture technique explained in Section 2.2. It indicates a total impact energy dissipation without reaching a complete separation of the fracture surfaces.

A general view of the sample (Fig. 5) shows three distinct zones:

(I) Razor blade notch front and initial crack propagation (in other terms the crack propagation roughly begins when the applied load reaches F_{max}, and the displacement corresponds to δ_{i}^*, see Fig. 2b).

(II) Fracture surface showing slow propagation guided by the hammer (corresponding to δ_{p} in Fig. 2b);

(III) Area of manual separation.

The increasing necking from zone (I) to (II) is a characteristic feature of this fracture propagation surface: in zone (I) a state of plane strain is still considerable due to the effect of the sharp notch; vice versa, in zone (II) a state of plane stress prevails.

Higher magnifications show the presence of further morphologically different areas, which can be distinguished proceeding from the notch tip towards the end of the fracture. The exact location of the details shown in Figs 6 to 9 is indicated by the corresponding numbers in Fig. 5 and in the following images taken at low magnifications. The arrows at the foot of each picture show the direction of crack growth.

Fig. 6 reports a detail of the fracture induction area; it is characterized by the razor notch tip and by lines starting from irregularities situated at the notch tip itself. Higher magnifications show neither further microstructures (cavitations, shear planes etc.) nor significant morphological differences from the central part of the induction area to the external sides.

Fig. 7 shows a magnified detail taken along the central axis of the fracture surface, about 0.8 mm from the notch tip. Its main feature is the appearance of slight shear bands intersecting at an angle of approximately 76°. They are superimposed on a system of lines parallel to the direction of crack growth.

Fig. 8a is taken at lower magnification in the central part of the fracture surface, at 1.5 mm from the notch tip. It points out a marked increase of shear bands, appearing no more rectilinear but set into a “fish-bone” appearance: the shear bands lie parallel to each other, slightly arched and converging from the sides towards the centre of the specimen, where they intersect.

Such an appearance must somehow reflect a continuous variation of the stress tensor from the outer side to the central axis of the fracture surface: anyhow this requires that constraint phenomena may occur, having varying intensities from the edges towards the inner part of the fracture surface.

Fig. 8b shows a magnified detail taken from Fig. 8a, at the intersection between shear bands with an angle of about 71°.

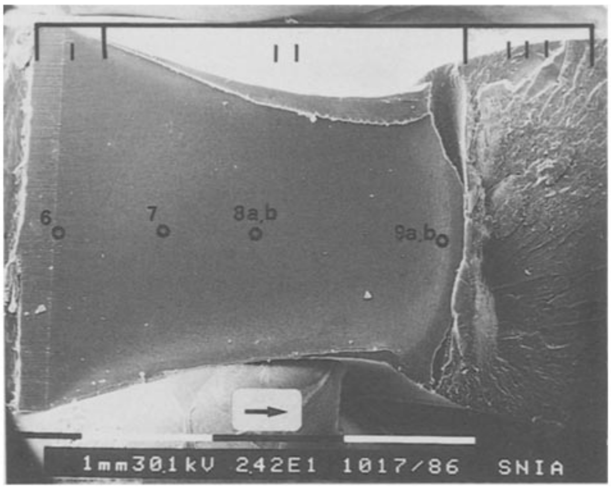

Figure 5 Water conditioned PA6 – comprehensive view of the (D) surface. The numbers show the loci of the following images – Figs 6 to 9. The arrow indicates the direction of crack growth.

---

*Fundamentally, crack propagation always begins before F_{max} has been attained. In the present case the degree of advancement is a secondary aspect if compared with the morphological evidence.

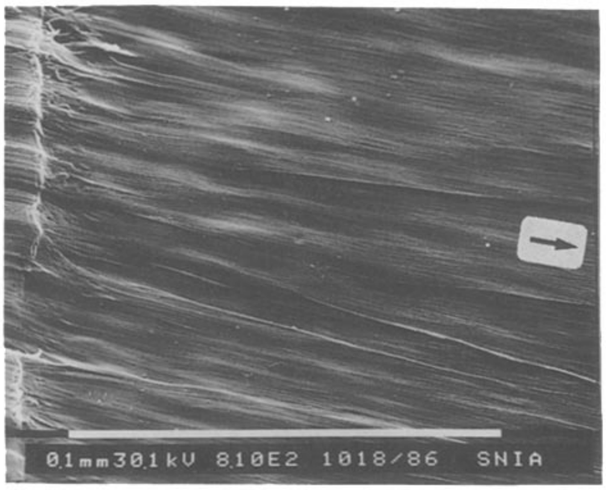

Figure 6 Water conditioned PA 6 – fracture induction. Razor blade notch tip, left.

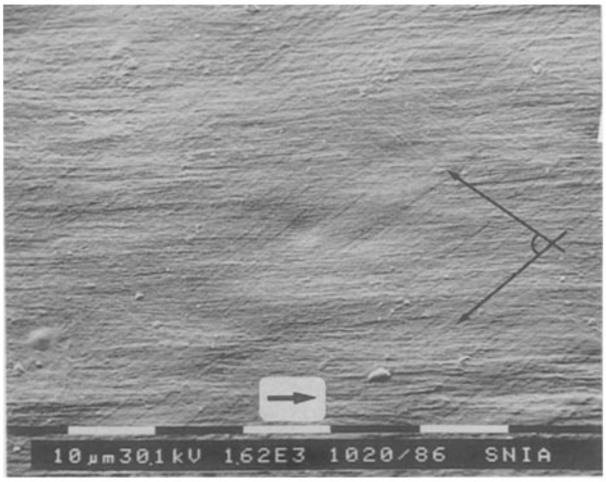

Figure 7 Water conditioned PA 6 – shear band appearance 0.8 mm from the notch tip. Shear bands intersect at about 76°.

A detail taken at about 2.9 mm from the notch tip is shown at different magnifications in Figs 9a and b; it represents the fracture morphology close to the limit of crack propagation (see also Fig. 5). An overlap is evident between the just mentioned "fish-bone" shear bands and the characteristic rumples set parallel to the crack advancement front. The appearance of rumples is probably caused by the changed stress conditions (strain speed tending to zero). Fig. 9b (which reports a central detail of Fig. 9a) clearly shows the additional presence of small secondary bands oriented both parallel and perpendicularly as to the front of crack growth. The whole system of shear bands and rumples fits for the construction of a deformation model based on shear planes, in agreement with the orientations of the edges of a regular octahedron.

In conclusion, Figs 5 to 9 tend to show that in water conditioned PA 6 the high impact energy dissipation is due to plastics shear; the presence of rumples, connected with particular tensile conditions, is an evidence of it.

3.2. Fractographic analysis of transversally cold-dissected HI-PA 6

Moulded test bars in HI-PA 6 were sharply notched and fractured at $T = 23°C$ by 3PB impact, in conformity with the details reported in Section 2.2. Then, transverse sections of the ductile fracture surfaces were obtained parallel to the (x, z) plane, by means of the technique described in Section 2.3. Fig. 2c shows the force–deflection curve referred to the impact test at room temperature. This behaviour is associated with high rate of plastic deformation and hence high energy dissipation developed during fracture. The resulting fracture surfaces showed both signs of necking (not so remarkable as in water conditioned PA 6) and stress whitening below the surface. Both witness the development of dissipative processes deeply inside the material.

In order to evaluate the nature of such processes and to quantify them, the secondary cryogenic fracture surface (parallel to the (x, z) plane) was scanned by SEM at various depths below the ductile fracture surface (parallel to the (x, y) plane). A comprehensive view of the fractured specimen is reported in Fig. 10. The ductile fracture surface D, is affected by necking; moreover also at low magnifications the rumples are visible and similar to those observed by Hahn *et al.* [6]. A detail is shown in Fig. 11a. Their regularity and periodicity (rumples always lie parallel to the crack advancement front) suggests they reflect somehow the fronts of shear bands. At greater magnifications

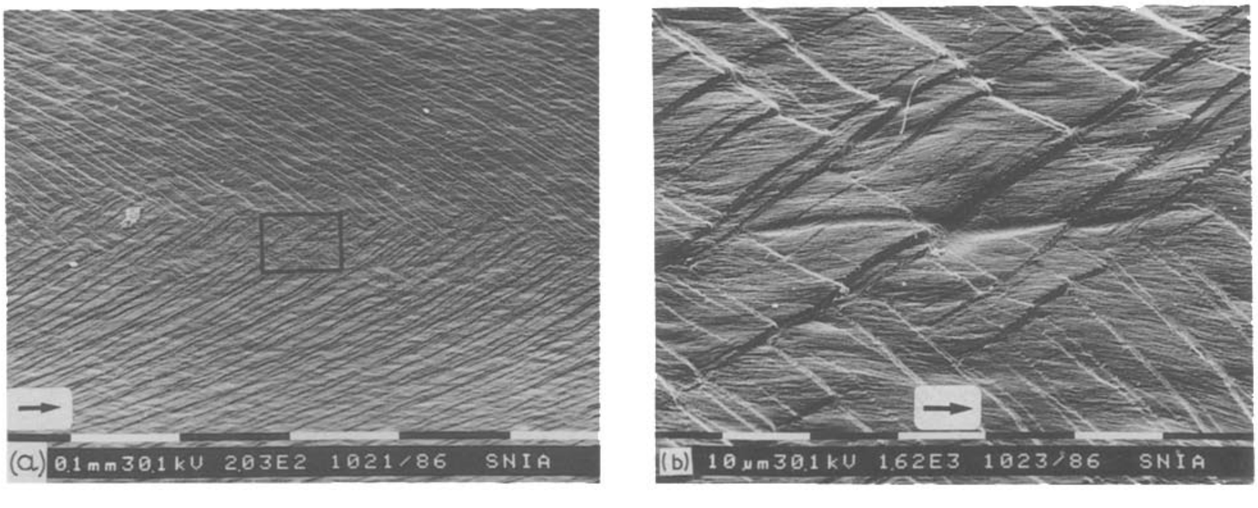

Figure 8 (a) Water conditioned PA 6 – "Fish-bone" shear bands at 1.5 mm from the notch tip. (b) higher magnification of the central area of (a).

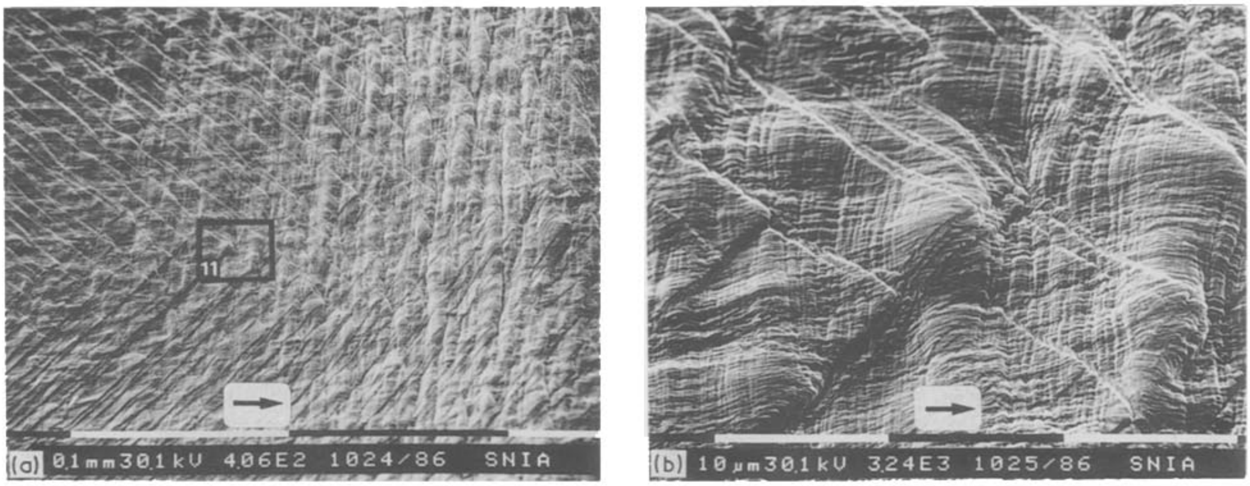

Figure 9 (a) Water conditioned PA 6 – morphology in proximity of the limit of crack propagation. Note the overlapped rumples and fish-bone bands. (b) Higher magnification of the central area of (a). Note the rumples developing both parallel and perpendicularly to the direction of crack growth.

(Fig. 11b) the surface morphology between rumples appear to be made by thin tufts of drawn material.

The cryogenic fracture surface is marked by B in Fig. 10. The figure shows the loci of four micrographs respectively taken at 1.2, 0.7, 0.35 and 0.1 m respectively from the DB edge formed by the intersection between the planes D and B. The corresponding images, taken at equal magnification (5000 ×) are shown in Figs 12a to d. They reflect the morphology of the stressed material behind the D surface. At least three remarks must be made

(a) A widest cavitation is present in the whitened volume.

(b) The intensity of cavitation varies depending on the depth under the D surface.

(c) Cavities show a tendency to grow along preferential fronts.

In fact the image taken at 1.2 mm depth (Fig. 12a) shows no signs of plastic deformation; the fast fracture only reveals undeformed rubbery particles, some of which (indicated with arrows) broke during fracture.

At 0.7 mm depth (see Fig. 12b) cavities are already evident. They concern only a part of the whole particles, and tend to develop along a preferential direction.

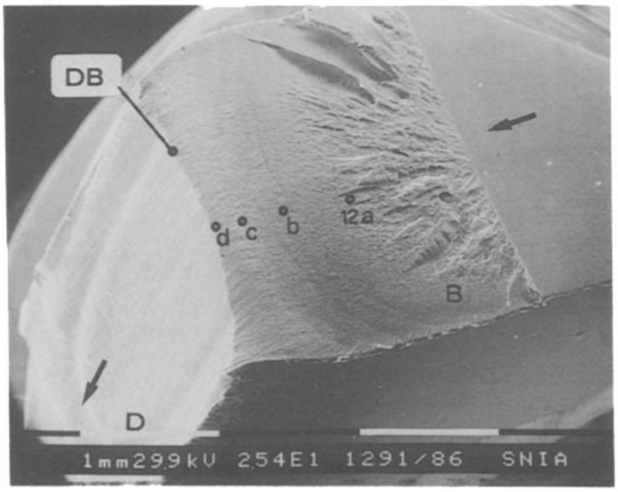

Figure 10 Transversally cold-dissected HI-PA 6 (TCD HI-PA 6) – comprehensive view ((D) = (x, y) ductile fracture surface; (B) = (x, z) brittle fracture surface; DB = D and B intersection).

The fractograph taken at 0.35 mm from the D surface (Fig. 12c) shows general cavitation and the total absence of visible rubbery particles. In this case, too, a certain alignment among cavities can be seen suggesting the presence of a system of shear bands.

The intensity of cavitation at 0.1 mm from the D surface is really remarkable (Fig. 12d). The structure of the material prevalently consists of voids surrounded by walls of drawn material. The huge dimension of some voids might be caused, at least partly, by coalescence between neighbouring cavities.

These observations give rise to two main conclusions.

(a) Cavitation around the rubbery particles is primarily an important dissipative mechanism during the ductile fracture of HI-PA 6. This is in agreement with the observations by Yee and Pearson [7, 8] according to which each dispersed rubber particle act as a nucleating agent for cavitation.

(b) Such an extensive void formation must necessarily require high deformation of the polyamide matrix by drawing or shear yielding.

Fig. 13 refers to unpublished work about the morphology of a HI-PA 66 sample having the same rubber type, content and morphology as the present HI-PA 6 samples, and transversally cold dissected with the present technique (see Fig. 4 – trans (x, z)). It shows the length distribution of the major axes for the elongated cavities, as a function of their distance from the DB edge. The values taken at 795 μm from DB coincide with the real mean diameters of the elastomeric domains and in fact traces of cavitation could not be detected at this depth, as the particles were undeformed.

Thus, in the proximity of the D surface, the material surrounding the rubbery particles undergoes 500 to 600% elongation by cavitation. The average diameter of the undeformed domains is about 0.6 μm (between 0.2 and 1.0 μm), while the major axis of cavities, considered is approximately elliptical, reaches on average

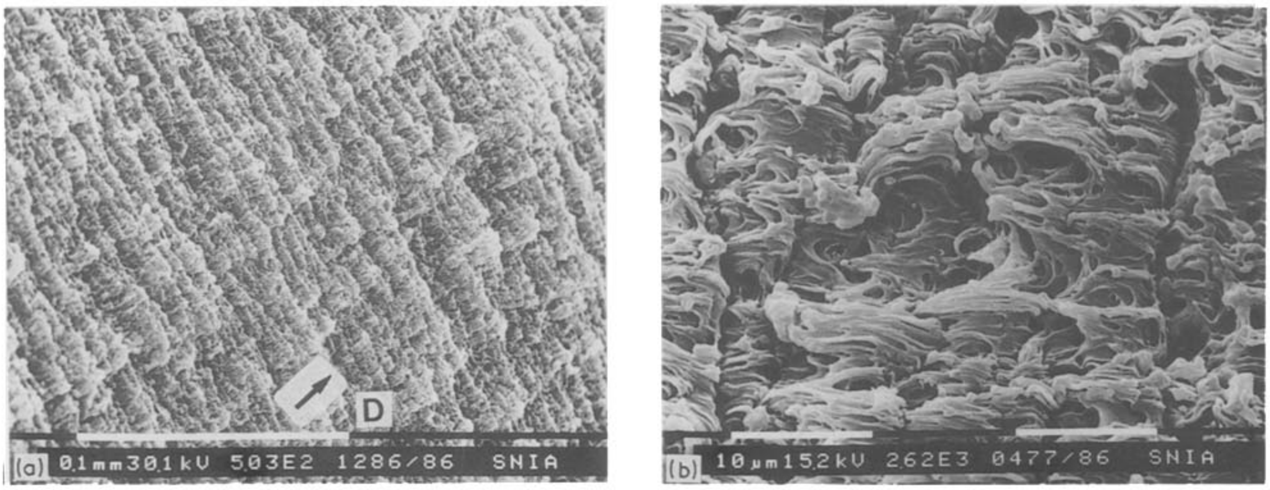

Figure 11 (a) TCD HI-PA 6 – D fracture surface, with extensive rumple development. (b) TCD HI-PA 6 – Higher magnification of rumples on the D surface. Tufts of drawn material are evident.

3 μm (from 1.6 to 5.5 μm) near DB, where drawing is maximum. Similar rates of elongation also occur in the transversally cold-dissected HI-PA 6 samples (see the particle and cavity size in Figs 12a to d).

On the other hand, similar cavitation phenomena around sites of discontinuity, in association with extensive plastic deformation, are well known in metallurgy [10, 18–21]. Some theories postulated years ago about ductile alloys reveal some important analogies with the presently described results.

In particular, one model derived by Backhofen [18] for metals agrees well with hypothesis that the drawn material tufts (clearly visible in Fig. 11b among the rumples) are the walls of the cavities, locally subjected to tensile stress beyond the break point.

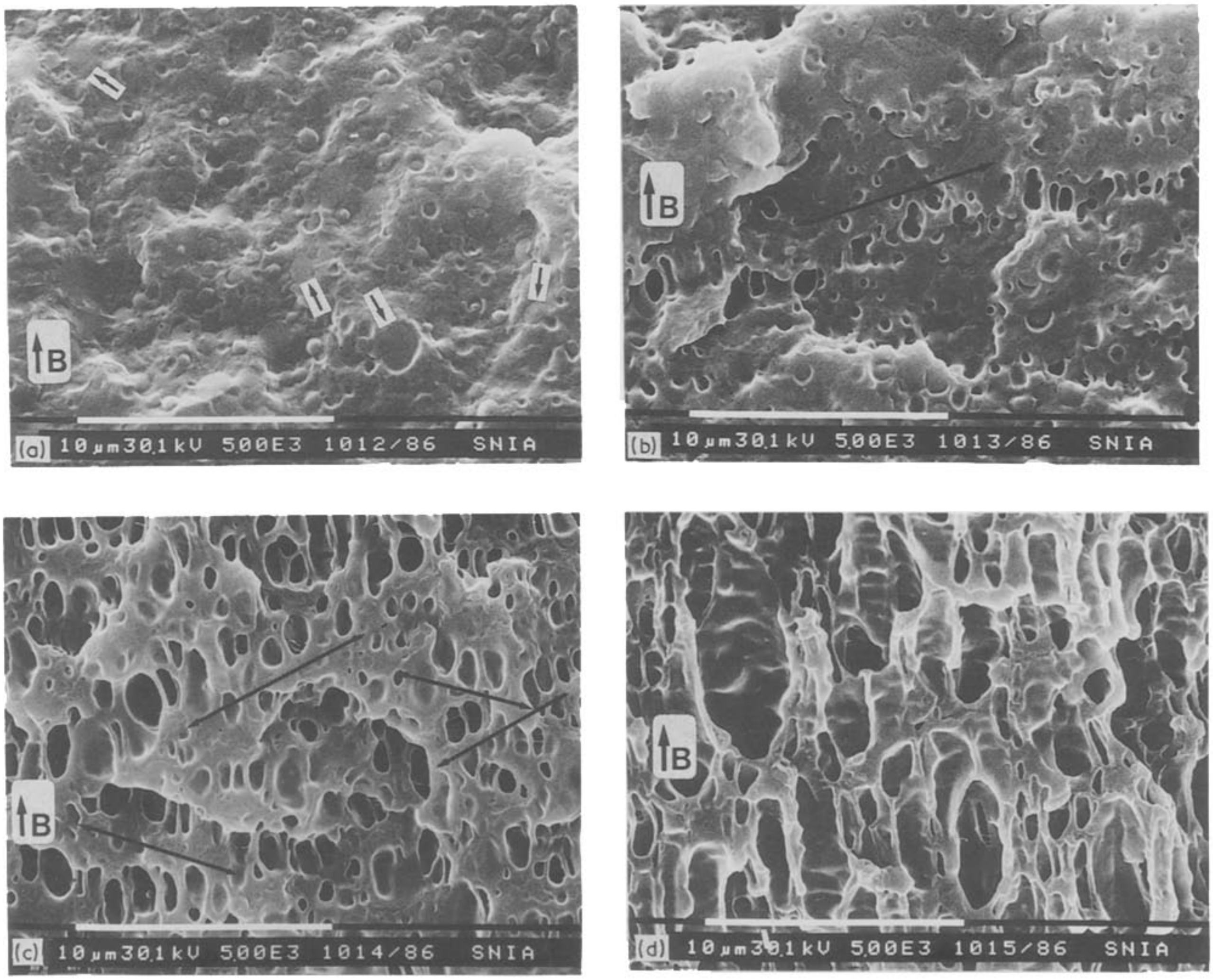

Figure 12 (a) TCD HI-PA 6 – morphology on the B surface 1.2 mm far from the DB edge. The arrows show some rubbery particles broken in a brittle way. (b) TCD HI-PA 6 – B surface 0.7 mm from DB. Note the orientation of the cavitation front. (c) TCD HI-PA 6 – B surface 0.35 mm from DB. Note the preferential orientations of cavitation fronts. (d) TCD HI-PA 6 – B surface 0.1 mm from DB.

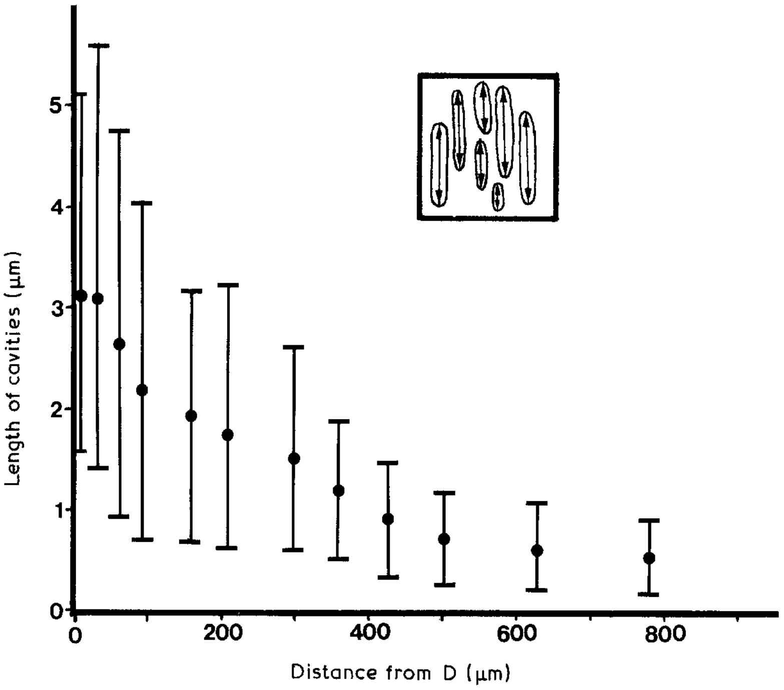

Figure 13 Size distribution of the elongated cavities (measured along their major axes) plotted against distance from D in a TCD HI-PA 6.6 sample.

3.3. Fractographic analysis of longitudinally cold-dissected HI-PA 6

Specimens consisting of HI-PA 6 were firstly impact tested at 23° C, the ductile fracture lying parallel to the (x, y) plane (see Section 2.2); then the fracture surface was cold-dissected parallel to the (y, z) plane, as described in Section 2.3 and shown in Fig. 4. The resulting brittle fracture was perpendicular to the rumples and parallel to the ductile crack growth direction.

A picture of the resulting specimens is reported in Fig. 14, where D and B are the ductile and brittle fracture surfaces, respectively, and the DB edge is their intersection. Figs 15 to 16 are fractographs taken on the B surface along a line normal to D, 0.8 mm from the limit of the razor blade sharp notch (see in Figs 14 and 15a the loci of such micrographs).

The morphology 0.4 mm below the DB edge is shown in Fig. 15b and only underformed rubber particles (or their prints) are present. In contrast a complex morphology appears closer to the DB edge. Fig. 15c, taken at about 0.2 mm from it (2100 ×) clearly shows the occurrence of generalized cavitations.

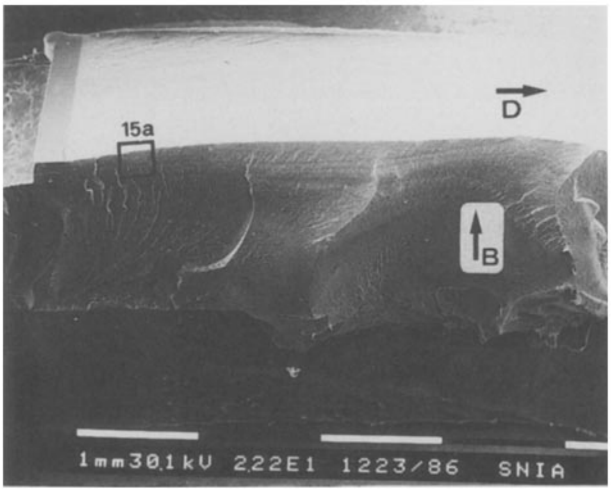

Figure 14 Longitudinally cold-dissected HI-PA 6 (LCD HI-PA 6): comprehensive view of the specimen.

At least partially, they seem to develop along fronts about 20° inclined with the plane of the D surface. Such a structure is even more evident in Fig. 15d, the picture being taken at 0.1 mm from DB where cavities are more marked (consider however that Fig. 15d is twice the magnification – 4200 × – as Fig. 15c). One can also observe both a preferential stretching direction for voids and their tendency to align along fronts inclined about 20° to the D surface. Such preferential directions (void stretching and void alignment) nearly intersect with an angle of 76°.

The morphology of the cavitated material 30 μm below the ductile surface is shown in Fig. 15e. Voids are highly stretched and oriented (mean sizes: 2.7 μm length; 0.4 μm width). This latest value is comparable with the mean diameters of the undeformed particles).

Finally, the structure of the B surface at the boundary with the DB edge is shown in Fig. 15f. The cavities are extremely oriented and inclined and also connected with the rumples lying on the D surface.

From these pictures it is evident that an association exists between cavitation around the rubber particles and an extensive shear of the PA matrix, occurring shortly before the separation of the ductile fracture surface. The oblique orientation of the voids to D surface cannot be explained otherwise. Furthermore, the angle included between the void stretching and void alignment directions – about 76° (see Figs 15d and e) – compares well with the angle at the intersection of shear bands already observed on the fracture surface of pure, water conditioned PA 6 (Figs 7 and 8).

It is also interesting to notice some long horizontal discontinuities clearly visible along the B surface in the present sample (see Fig. 15a). At higher magnifications (Figs. 15c, 16a, b) they are revealed as long slits marked by an evident drawing-to-break of the matrix around the cavities. The orientation of threads

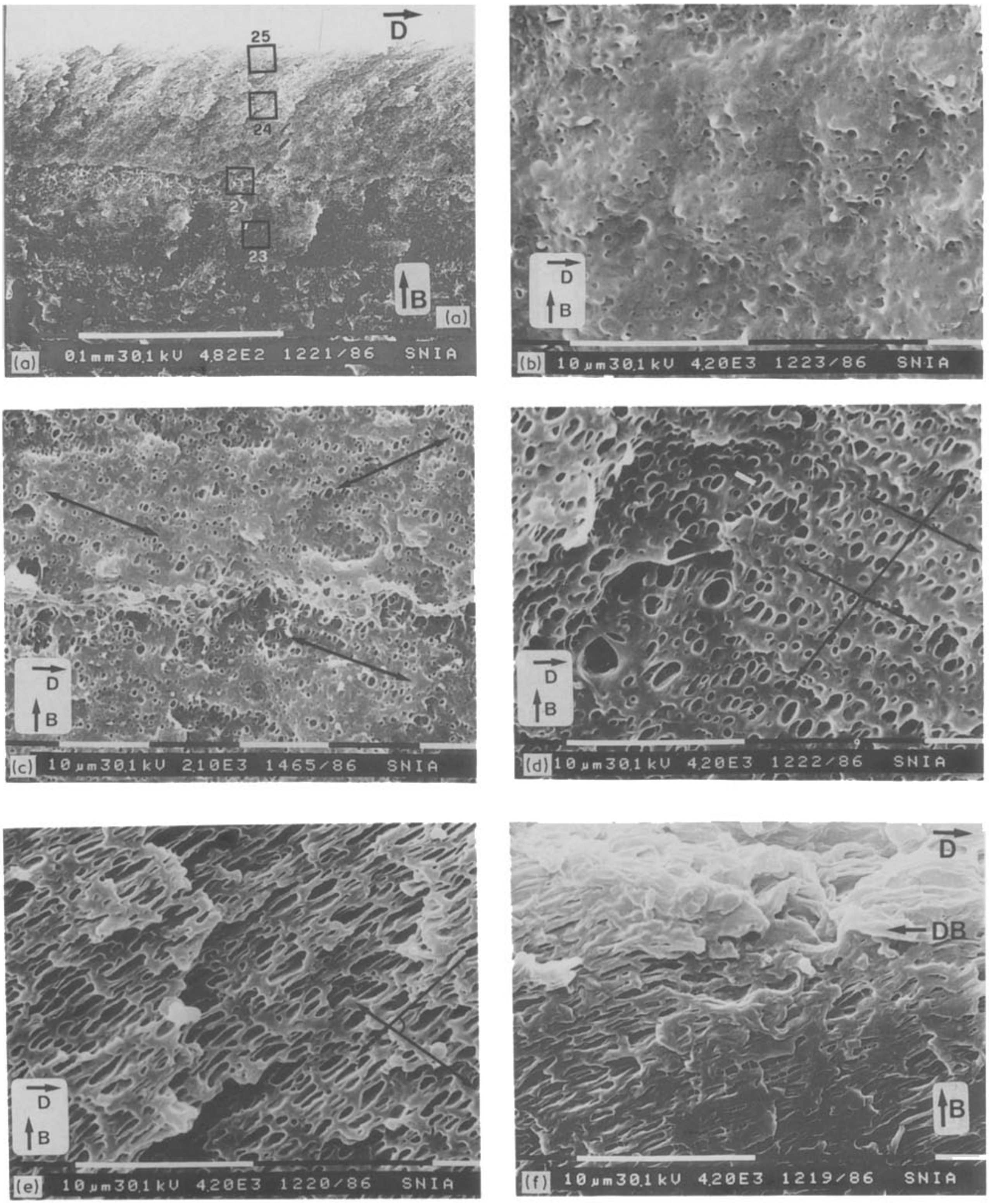

Figure 15 (a) LCD HI-PA 6 – Morphology of the B (y, z) surface near the D (x, y) surface: comprehensive view. (b) 0.4 mm from DB, (c) 0.2 mm from DB. Note the cavitation fronts and the long horizontal discontinuity. (d) 0.1 mm from DB. The angle is marked between the alignment direction of cavitation fronts and the draw direction of voids. (e) 30 μm from DB. (f) close to DB. The D surface is visible at the top of the picture.

also seems to be totally different if compared with that of the neighbouring cavitated particles outside the discontinuities (Fig. 16a). Such a morphology can be regarded as being caused by shear along oblique planes to the D surface and parallel to the x axis.

In conclusion, the SEM analysis of a longitudinally cold-dissected sample shows shear deformations developed along several preferential planes, caused by impact testing in ductile conditions. Such orientations are sketched in Fig. 17. The α plane represents the orientation of the cavitation fronts. The β plane presumably represents the longitudinal shear bands (discontinuities) shown in Figs 15c and 16a, b. The γ plane corresponds to the drawing orientation of the voids.

Further preferential shear and cavitation direction could be revealed by a comprehensive fractographic analysis. As already stated, they should be consistent

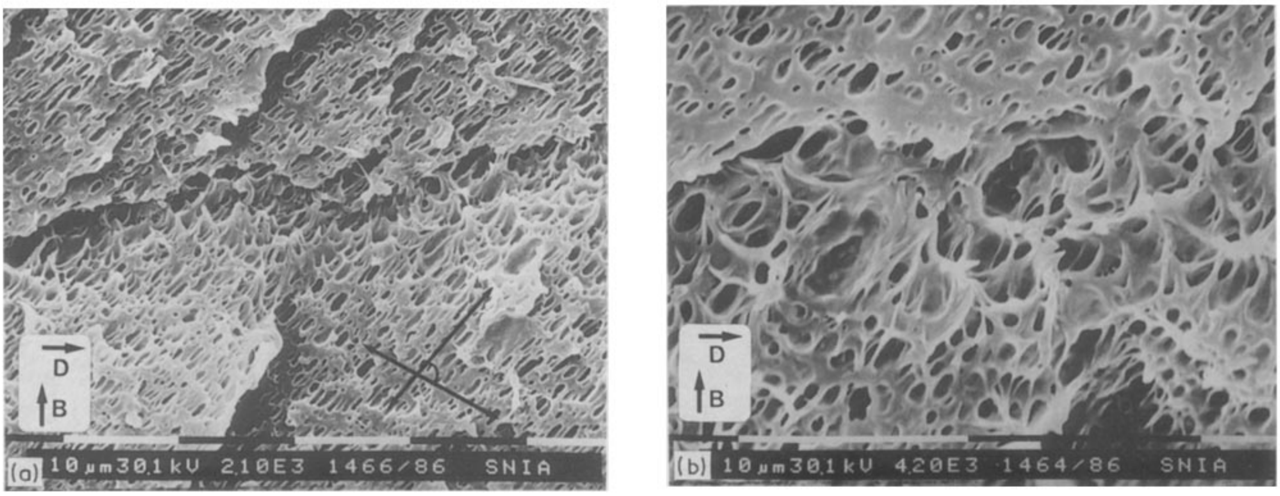

Figure 16 LCD HI-PA 6 (a) Horizontal discontinuity. Note the different draw direction of voids in comparison with the neighbouring material. (b) Higher magnification of a discontinuity band (70 μm from DB).

with the theoretical considerations regarding deformations along the octahedral shear planes.

4. Discussion

In our opinion the present fractographic analysis univocally defines, even if not quantitatively, the dissipative mechanisms involved during the ductile fracture propagation in rubber toughened polyamides. A particular aim of this work consisted in determining if the rumpled fracture surface morphology [4–6] was caused by matrix shear yielding and/or if evidence of further dissipative mechanisms could be recognized by fractography.

A preliminary SEM analysis was performed on water conditioned PA 6 ductile fracture surfaces, obtained by Charpy impact testing with a sharp notch. In such conditions shear yielding resulted as the prevailing dissipative mechanism during crack growth. Moreover, rumples were associated with shear band spacing.

The orientation of shear bands is affected by the local stress conditions (state of plane stress or plane strain; local crack speed distance from the notch or from the borders). For this reason shear bands can result either spaced and oblique ("fish-bone" structure) or dense and parallel or perpendicular to the crack growth front, according to the local geometry and stress conditions of the specimen. Their typology well fits the models for shear yielding along octahedral planes, typical of ductile materials and well known by metallurgists [9, 10, 18–21].

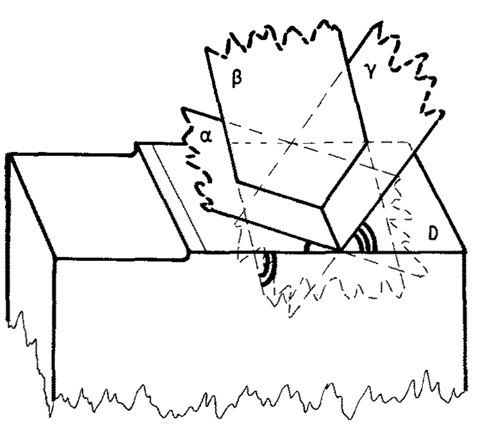

Figure 17 Schematic picture of the main observed orientations caused by ductile deformation in HI-PA specimens (α = cavitation fronts: β = horizontal separation planes; γ = draw fronts).

From these results we supposed that also in rubber toughened polyamides the ductile fracture propagation could be due to matrix shear yielding induced by the presence of finely dispersed rubber particles. A SEM investigation about the state of deformation in the region below the fracture surface was necessary in order to verify these assumptions and to correlate rumples with viscous shear phenomena, according to the octahedral shear theory. The simple technique used to cold-dissect the specimens normally to the ductile fracture surface allowed the analysis of their internal morphologies to be achieved. The stress whitened regions are largely ruled by shear yielding of the polyamide matrix and by an extensive cavitation around the discrete elastomeric phase. From the reported pictures a tendency is evident to develop cavitation fronts involving neighbouring and aligned particles. Around them the matrix undergoes remarkable drawing, the closer the matrix to the ductile, D, fracture surface, the higher the drawing.

Furthermore, the drawing direction of cavities and the growth direction of cavitation fronts intersect according to angles comparable with the ones formed by shear bands intersecting on the fracture surfaces of water conditioned PA 6.

We can believe that shear yielding and cavitation are mutually correlated and the presence of rubbery particles acting as stress concentrators lowers the local σ_Y (nominal) of the matrix [22–24]. Rumples are a consequence of yielding mechanisms along shear bands. The SEM fractography of longitudinal and transversal, B surfaces, taken immediately beneath the D fracture surfaces (see Fig. 15f) shows rumples connected with shear planes developing inside the stress whitened volume. Shear planes appear inclined as to the (x, y) plane of the ductile fracture surfaces, but also parallel to the front of crack growth. Their orientation coincides with the orientation of cavities occurring beneath the ductile surfaces (see Fig. 15e).

On the other hand the presence of shear planes with further orientations, not necessarily coinciding with rumples, is suggested by a deeper observation of the inner morphology of specimens (see Figs 15c, e and 16a). This hypothesis is strengthened by analysis of the fracture surface of water conditioned PA 6. The development of preferential orientations for octahedral shear bands and shear planes strongly depends on the local geometry and stress conditions.

The combination between shear yielding and cavitation as dissipative mechanisms during impact quite well agrees with the model proposed by Hahn *et al.* [6] to explain the nature of the rumples. Furthermore, it almost coincides with Yee's arguments [7, 8] about the dissipative mechanisms in epoxy–rubber blends where an analysis by SEM and by polarized optical microscopy revealed the presence of both shear bands and cavitations around rubber particles. Yee also suggested that toughening is mainly due to notch blunting caused both by shear yielding and cavitation of the material immediately surrounding the crack tip. The phenomenon would take place before the crack opening and would keep nearly steady during propagation, as also evidenced by the regularity in rumple spacing on the ductile fracture surfaces.

Moreover, some SEM fractographs of longitudinally cold-dissected HI-PA 6 samples – not reported in the present work – showed the development of extensive cavitation and shear fronts immediately around the notch tip. The cold-dissection technique described in this work would easily allow a morphological analysis of specimens stressed below the break limit. Thus, it could be possible to verify the state of a partially deformed material in proximity of the stress concentrator.

The observed extensive cavitation also strengthens Wu's theory [15] considering the interparticle distance between the rubbery domains as the critical parameter for the establishment of a ductile behaviour within a wide range of testing conditions. In fact a strong interaction between the stress fields surrounding neighbouring particles [11] promotes the growth of cavitation fronts and of shear bands inside the continuous polyamide phase. Finally, it is worth emphasizing that for the first time the morphology of the deformed material below the "natural" fracture surface is systematically shown. By induction, this state reflects the state of plastic deformation existing inside the material immediately before the local fracture propagation. The significance of the present analysis is based upon the assumption that the state of the deformed specimen after ductile fracture is not altered by the following cold-dissection.

References

1. A. G. ATKINS and Y. W. MAI, *J. Mater. Sci.* **21** (1986) 1093.
2. M. I. KOHAN, "Nylon Plastics" (Wiley Interscience, New York, 1973) p. 318.
3. C. GARBUGLIO, G. AJROLDI, T. CASIRAGHI and G. VITTADINI, *J. Appl. Polym. Sci.* **13** (1971) 2487.
4. E. A. FLEXMAN, *Kunststoffe* **69-3** (1979) 172.
5. M. T. HAHN, R. W. HERTZBERG, and J. A. MANSON, *J. Mater. Sci.* **21** (1986) 31.
6. *Idem., ibid.* **21** (1986) 39.
7. A. F. YEE and R. A. PEARSON, *J. Mater. Sci.* **21** (1986) 2462.
8. R. A. PEARSON and A. F. YEE, *ibid.* **21** (1986) 2475.
9. A. NADAI, "Theory of Flow and Fracture of Solids" (McGraw-Hill, New York, 1950).
10. A. S. TETELMAN and A. J. McEVILY, Jr, "Fracture of Structural Materials" (Wiley, New York, 1967) p. 50.
11. S. Y. HOBBS, R. C. BOPP and V. H. WATKINS, *Polym. Eng. Sci.* **23** (1983) 380.
12. F. RAMSTEINER, *Kunststoffe* **73-3** (1983) 148.
13. F. RAMSTEINER and W. HECKMANN, *Polym. Commun.* **26** (1985) 199.
14. S. WU, *J. Polym. Sci. Polym. Phys. Ed.* **21** (1983) 699.
15. *Idem., Polymer* **26** (1985) 1855.
16. F. IDE and A. HASEGAWA, *J. Appl. Polym. Sci.* **18** (1974) 963.
17. F. POLATO, *J. Mater. Sci.* **20** (1985) 1455.
18. W. HAYDEN, W. G. MOFFATT and J. WULFF, "The Structure and Properties of Materials" Vol. III (Wiley, New York, 1965) § 7.5 Fig. 7.6.
19. B. R. LAWN and T. R. WILSHAW, "Fracture of Brittle Solids" (Cambridge University Press, Cambridge, 1975) § 2.4 pp. 39–41.
20. R. F. SMITH and J. F. KNOTT, "Conference Proceedings Practical Application of Fracture Mechanics to Pressure Vessel Technology" (Institute of Mechanical Engineers, Cambridge University Press, Cambridge, 1971) p. 65.
21. J. F. KNOTT, Fundaments of Fracture Mechanics" (Butterworths, London, 1979) p. 215.
22. A. L. GURSON, *J. Eng. Mater. Tech. Trans. ASME* **99** (1977) 2.
23. H. YAMAMOTO, *Int. J. Fracture* **14** (1978) 347.
24. V. TVEERGARD, *ibid.* **17** (1981) 389.

Received 18 August 1987
and accepted 27 July 1988